This is an open access article published under an ACS AuthorChoice License, which permits copying and redistribution of the article or any adaptations for non-commercial purposes.

analytical chemistry

Article

pubs.acs.org/ac

Rectangular Ion Funnel: A New Ion Funnel Interface for Structures for Lossless Ion Manipulations

Tsung-Chi Chen, Ian K. Webb, Spencer A. Prost, Marques B. Harrer, Randolph V. Norheim, Keqi Tang, Yehia M. Ibrahim,* and Richard D. Smith*

Biological Sciences Division, Pacific Northwest National Laboratory, Richland, Washington 99352, United States

Supporting Information

ABSTRACT: Structures for lossless ion manipulations (SLIM) have recently demonstrated the ability for near lossless ion focusing, transfer, and trapping in subatmospheric pressure regions. While lossless ion manipulations are advantageously applied to the applications of ion mobility separations and gas phase reactions, ion introduction through ring electrode ion funnels or more conventional ion optics to SLIM can involve discontinuities in electric fields or other perturbations that result in ion losses. In this work, we developed and investigated a new funnel design that aims to seamlessly couple to SLIM at the funnel exit. This rectangular ion funnel (RIF) was initially evaluated by ion simulations, fabricated utilizing printed circuit board technology, and tested experimentally. The RIF was integrated to a SLIM-time of flight (TOF) MS system, and the operating parameters, including RF, DC bias of the RIF electrodes, and electric fields for effectively interfacing with a SLIM, were characterized. The RIF provided a 2-fold sensitivity increase without significant discrimination over a wide m/z range and well matched to that of SLIM, along with greatly improved SLIM operational stability.

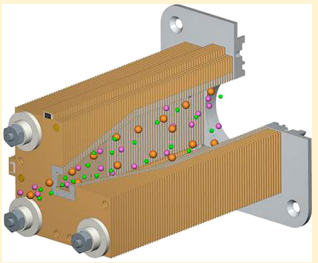

Electrospray ionization mass spectrometry (ESI-MS) is widely applied for studying chemical and biological samples ranging from small organic compounds to large biomolecules.[1−4] An ESI source nebulizes sample solutions to create highly charged fine droplets that evaporate to form ions, often as the droplets travel to the much lower pressure regions of the mass spectrometer (MS).[5,6] A variety of ion optic approaches to transfer of ions through a conductance limiting aperture to lower pressure regions from the typically 1−10 Torr interface region have been developed, including skimmers,[7] multipole ion guides,[8] and ion funnels.[9−13] A skimmer, typically installed between the end of the inlet orifice or capillary and a multipole ion guide to serve as a gas conductance limiting orifice, is generally designed to sample only ions located inside of a Mach disk of a supersonic free-jet expansion and, thus, only samples a limited portion of the ions, biased toward the heavier ions[10,14,15] Both RF multipole ion guide and stack-ring electrodes, with different phases of RF applied to adjacent electrodes, can be used to confine ions and increase transmission in these regions.[16,17] The electrodynamic ion funnel is an early implementation of such approaches that can efficiently sample and focus widely dispersed ions into a small radius for transmission through a conductance limiting aperture for downstream ion manipulation or mass analysis.[18−20] The effective potential from ring electrodes is steep near the electrodes but weak near the central axis of the rings, which creates a larger acceptance than the ion emittance area and which maximizes ion capture efficiency.[16] Major gains in ESI-MS sensitivity, for example, have been achieved by using ion funnels, as well as in coupling ion mobility separations (IMS) with MS in order to improve the sensitivity and throughput for many bioanalytical applications.[21−26] For ultrasensitive IMS-MS, a multiple-stage ion funnel can be used to provide ion transfer and focusing prior to the drift tube.[11,27] The effects of thermal diffusion and Coulomb repulsion spatially broaden ion clouds while they traverse the drift region.[11] An exit ion funnel can thus be employed after the drift tube to refocus the ion packets for further improving IMS-MS sensitivity.[21]

Recently, structures for lossless ion manipulations (SLIM) have been developed and initially demonstrated for a range of ion manipulations, including ion mobility separations, ion trapping, and switching of ions between different paths.[28,29] The SLIM have been initially implemented by fabrication of small components that can then be assembled in a flexible fashion to enable more complex ion manipulations and in ways previously impractical. The initial SLIM components were fabricated using printed circuit board (PCB) technology by directly depositing arrays of "rung" and "guard" electrodes on two parallel planar surfaces. An appropriate combination of RF and DC fields was applied to the rung electrodes and DC-only field to the guard electrodes for ion confinement and control inside SLIM.[30,31] Each of these initial SLIM components consists of a planar central rung and outer guard electrodes on the PCB surface. Static DC voltages are applied to both rung and guard electrodes with additional RF voltage coupled to rung electrodes 180° out of phase with neighboring rungs, to provide radial confinement.

Received: September 23, 2014
Accepted: November 16, 2014
Published: November 19, 2014

 © 2014 American Chemical Society

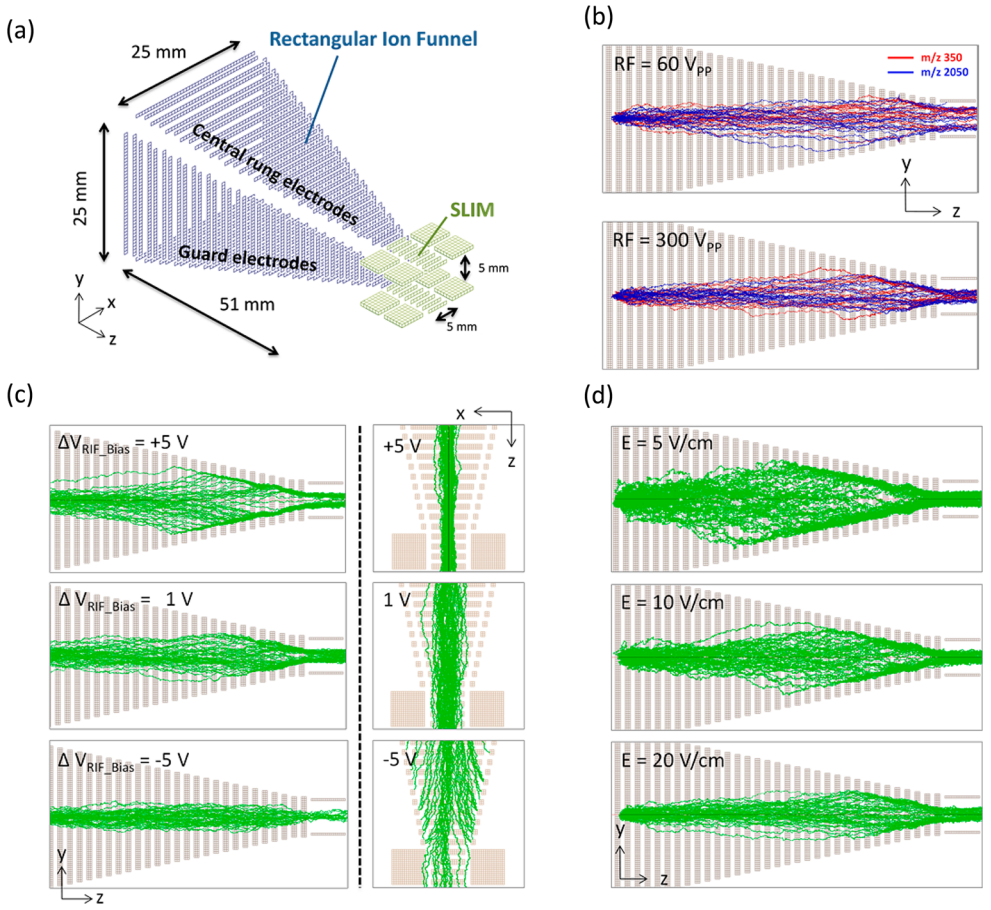

Figure 1. (a) Geometry and dimensions of RIF and SLIM entrance electrodes used in simulations. (b–d) Results for ion trajectories through the RIF showing the effect of: (b) RF amplitudes, (c) DC biases, and (d) DC gradients. The DC bias was defined as the voltage difference between the guard electrode and the central rung electrode. See text for the details of the ion simulations.

In one initial study, ions were introduced from a previously developed ion funnel trap (IFT) to an IMS module fabricated from linear path SLIM components followed by an exit ion funnel for interfacing with a time of flight (TOF)-MS.[28] While lossless ion transmission in the SLIM module was achieved, ion losses at the IFT–SLIM interface were observed. Potential reasons for these losses include differences in the m/z ranges for effective confinement by IFT and the SLIM, respectively, as well as the potentials generated at the exit orifice of IFT (a 3 mm i.d. orifice) that do not match well to the SLIM entrance having a rectangular electrodes arrangement of approximately 5.0 × 4.5 mm.

In this work, we designed and evaluated a new rectangular ion funnel (RIF) interface to SLIM, and its integration into a IFT–SLIM-TOF-MS instrument. The performance and ion transmission were evaluated, and we show that significant gains in sensitivity were achieved.

EXPERIMENTAL DESIGN

Materials. Agilent ESI-L low concentration tuning mix (Agilent Technologies, Santa Clara, CA) was used to produce ions with m/z range from 118.09 to 2721.89 in ESI positive mode for RIF optimization and the sensitivity evaluation.

Ionization Source. The electrospray ionization (ESI) source used in this study consisted of a chemically etched emitter[32] (20 μm i.d.) connected to a 75 μm i.d. fused-silica capillary (Polymicro Technologies, Phoenix, AZ) through a zero volume stainless steel union (Valco Instrument Co. Inc., Houston, TX). A syringe pump (Fusion 100, Chemyx Inc., Stafford, TX) with a 250 μL syringe (Hamilton, Reno, NV) was used to infuse solutions at a flow rate of 300 nL/min. An ionization voltage of 3 kV (relative to the inlet capillary voltage) was applied to the stainless steel union.

Ion Sampling Interfaces. Positive ions generated from ESI were introduced through a heated capillary (140 °C) into a tandem ion funnel interface consisting of an ion funnel trap (IFT) followed by a RIF. The ion funnel trap was operated only in the continuous mode in this study and thus has the properties essentially identical to a conventional ion funnel. The two ion funnels were operated as follows: ion funnel trap RF 150 V$_{pp}$ at 800 kHz; IFT DC gradient at 15 V/cm; RIF RF frequency at 800 kHz. The inlet capillary was offset 9.3 mm from the IFT centerline to reduce any gas dynamic effects in the RIF.

Acquisition. MS data was acquired using MassHunter software (Agilent Technologies, Santa Clara, CA) utilizing three replicates to calculate the mean and the standard error.

RESULTS AND DISCUSSION

Ion Simulations. The electrode design of the RIF was guided by ion simulations prior to fabrication. The simulations of ion trajectories within the RIF utilized SIMION 8.1 (Scientific Instrument Services, Inc., Ringoes, NJ) with the SDS (statistical diffusion simulation) user program to model

dx.doi.org/10.1021/ac503564c | Anal. Chem. 2015, 87, 716–722

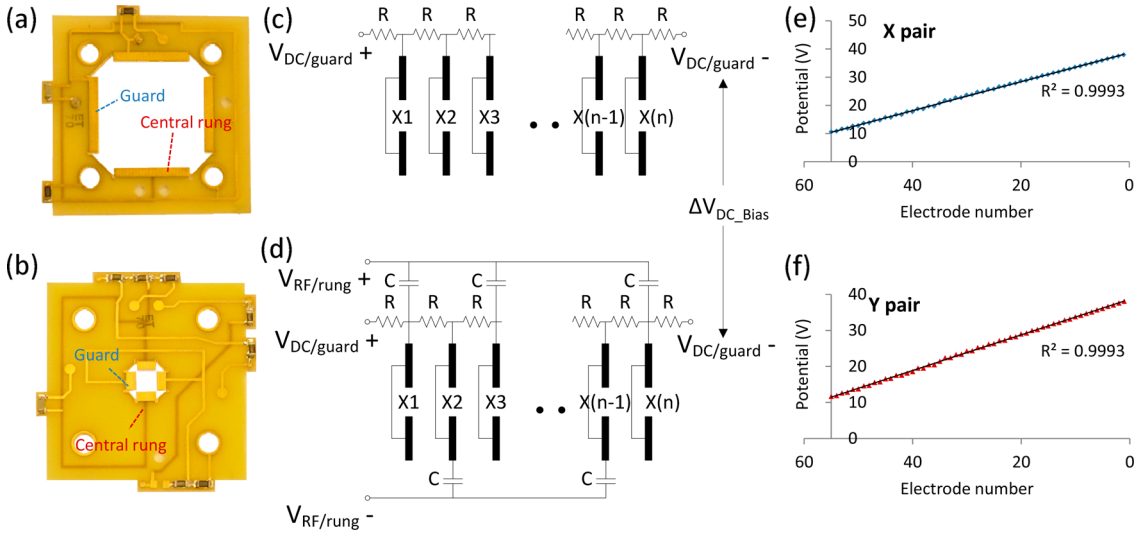

Figure 2. Design and fabrication of the PCB-based rectangular ion funnel. In the photos of (a) the first and (b) the last element of RIF, two pairs of the rectangular electrodes are connected to other electrodes on the adjacent elements based on the circuit layouts for the (c) guard/*x*- and (d) rung/*y*-pair to form (e and f) two independent DC gradients along RIF. Capacitors in (d) are used in RF coupling and DC blocking for the series of the central rung electrodes.

the effects of collisions of charge particles (mass range of m/z 50−2050) with background nitrogen molecules gas at a 4 Torr environment. In contrast to the conventional ion funnel designs using ring electrodes, the RIF utilizes 2 pairs of planar electrodes which form a rectangular outlet to better match the rectangular SLIM entrance dimensions. As shown in Figure 1a, the RIF entrance was designed with entrance dimensions of 25.0 × 25.0 mm, 5.0 × 5.0 mm for the exit, and 50.9 mm for the length of the RIF converging section. The 34 electrodes used in the simulation were 0.76 mm thick and spaced 0.76 mm apart. For optimum interfacing, the electrical fields applied to RIF are made similar to SLIM. Similar to the SLIM electrodes, the rectangular electrodes on each element (lens) include a pair of central electrodes in the *y* direction with superimposition of DC and RF voltages and a pair of guard electrodes in the *x* direction with DC-only voltages. The field continuity provided by the optimized voltages (Figure S1, Supporting Information) is expected to provide smooth ion transmission through the RIF−SLIM interface.

The design was first evaluated with simulations by introducing a wide range of ions (m/z 50−2050, in 200 m/z steps with 5 ions for each m/z) at the RIF entrance to model the effect of RF confinement and without considering effects due to excessive space charge. The ion motion was monitored for different RF parameters, particularly at the RIF−SLIM junction. In Figure 1b, selected ion trajectories of m/z 350 and 2050 ions are illustrated (in red and blue, respectively) with RF frequency at 800 kHz and electric field at 20 V/cm. The DC bias of the guard electrodes relative to the RIF central rung electrodes was set to 1 V ($\Delta V_{RIF\_bias} = V_{guard} - V_{rung}$), while the SLIM guard bias was set to 5 V (as optimized previously).[28] The ion trajectories remain primarily within the confining region of the RIF and SLIM electrodes with RF amplitudes ranging from 60 to 300 V_{pp}. The results showed that higher RF amplitudes are necessary to focus higher m/z ions, e.g., the ions of m/z 2050 (the blue trajectories, Figure 1b). The effective potential (V^*) for the averaged motion of ions in the fast oscillatory field can be described as[16]

$$V^* = \frac{q^2 E_0^{\,2}}{4m\Omega^2}$$

where E_0 is the amplitude of the oscillatory field, q and m are ion charge and mass of the ion, and Ω is the angular frequency of the oscillatory field. Accordingly, heaver ions experience less RF confinement which results in weaker ion focusing for higher m/z ions.

The ion distribution profile in the *xy* plane can be optimized by adjusting DC penetrations in the ion drifting area. To evaluate the effect of the guard DC bias on the ion transmission, the simulation was performed under the conditions of RF amplitude at 300 V_{pp} and frequency at 800 kHz and electric field strength at 20 V/cm for RIF. The results in Figure 1c show the ions were dispersed in the *y* direction for a positive DC bias at 5 V, dispersed in the *x* direction for a negative 5 V DC bias, and near equally dispersed in both directions for 1 V bias. The effect of the DC gradient was also explored in the simulation in order to optimize the electric field for the RIF. In the simulations, the operating parameters for the RIF and SLIM were fixed at RF 300 V_{pp} and 800 kHz, while the guard DC biases for the RIF and for SLIM were 1 and 5 V, respectively. The DC gradient applied on the central rung electrodes was varied from 5 to 20 V/cm. The results of the simulations (Figure 1d) indicated better transmission of ions for DC gradients of 10−20 V/cm. Some ion losses were observed at an electric field below 10 V/cm, presumably due to diffusion and/or space charge effects.[11]

RIF Design and Fabrication. Figure 2a,b shows the images of the RIF entrance and exit lens, respectively, fabricated utilizing PCB technology. Each lens has two electrode pairs forming a rectangle shape laid down on a thin dielectric material. As mentioned above, RF and DC are superimposed on one pair (rung electrodes) while only DC is applied to the other pair (guard electrodes). The electrodes are gold-plated copper material with a thickness of 50 μm and 2.0 mm wide. The RIF lenses are 0.76 mm thick and spaced 0.76 mm apart in the *z* direction to match the current electrode dimensions used in SLIM. The first 21 lenses have a constant electrode

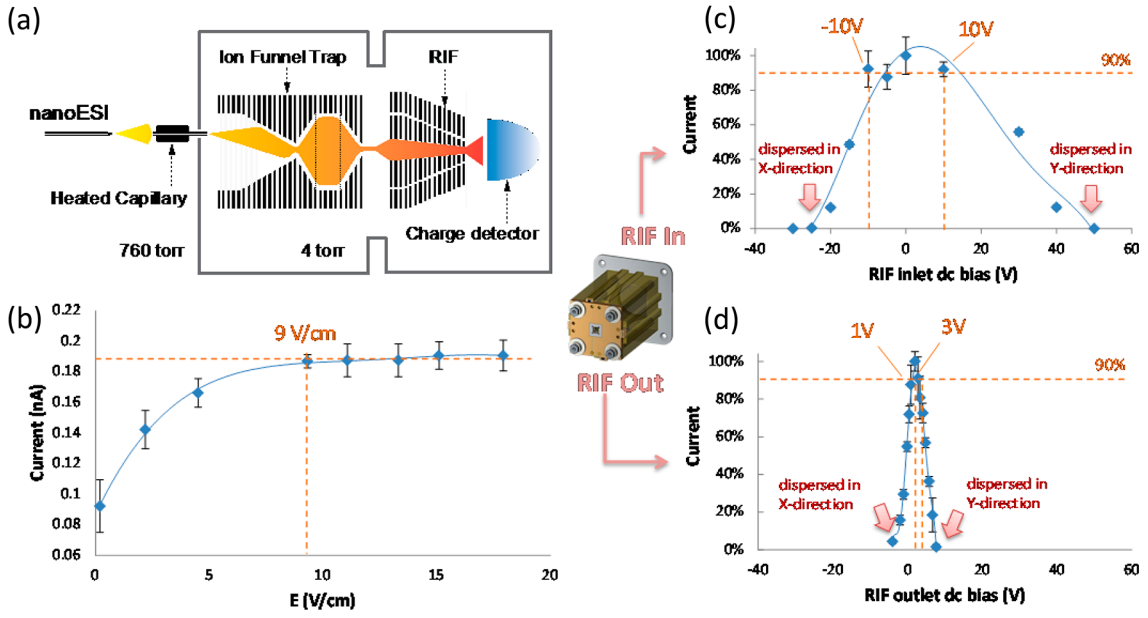

Figure 3. RIF characterization. (a) Schematic of the IFT-RIF arrangement. Ion current was measured as a function of (b) electric field, (c) DC bias at RIF inlet, and (d) DC bias at RIF outlet. The ion current was measured by a charge collector after the RIF exit at 4 Torr nitrogen using an ESI tune mix. The rung DC gradient was set at 9 V/cm for data shown in panels (c) and (d).

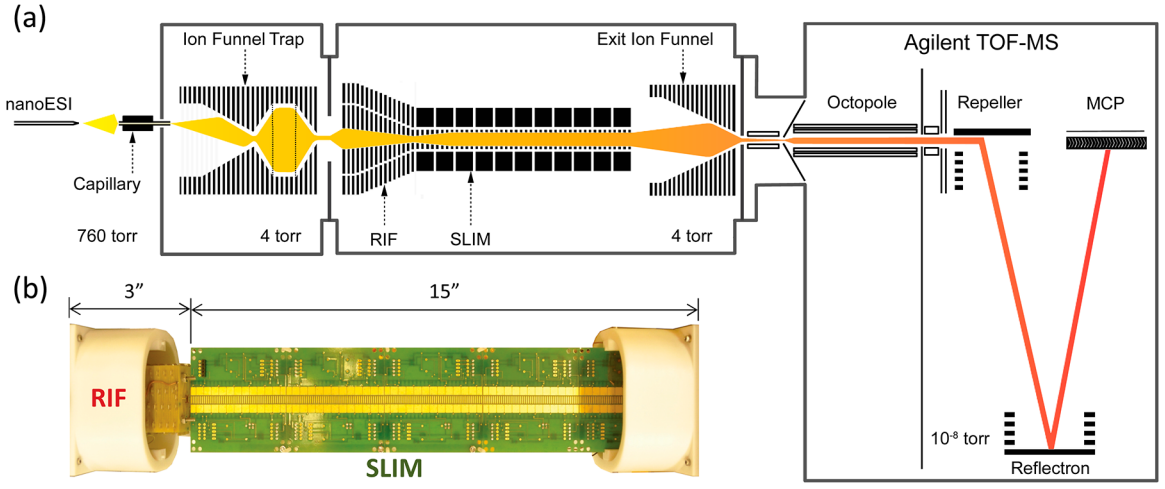

Figure 4. Details of the instrument design. (a) A representative schematic of the instrument used for the overall system performance evaluation. (b) Photo showing the RIF and SLIM module.

separation in a dimension of 25.0 × 25.0 mm (in x and y directions), and the last 34 lenses dimensions decrease linearly from 25.0 × 25.0 mm to 5.0 × 5.0 mm, forming an overall ~83 mm-long device.

The guard electrodes (x-pair) on each element are connected to a DC power supply while the central rung electrodes (y-pair) on the same lens are supplied with the superposition of a DC voltage and a RF waveform. Adjacent rung electrodes on subsequent lenses in the axial direction have a RF waveform of equal amplitude but opposite phase to produce RF ion confinement in the y-direction. The DC voltages applied on RIF gradually decreases toward the exit of the funnel to drive ions along the axial direction (z). Figure 2c,d shows the electronic circuit layout used to supply the DC and RF while Figure 2e,f shows the measured voltage of the dc potential on x- and y-pairs. The linearity of the electrode potentials minimizes field imperfections which may cause unpredicted ion motion and losses.

RIF Characterization. A schematic of the instrument arrangement used to characterize the RIF is shown in Figure 3a. The RF for the RIF was maintained at 160 V_{pp} at 800 kHz, and the guard DC bias was set at 3 V for the entrance lens and 1 V for the exit lens. A charge collector was placed at the exit of the RIF to evaluate the ion transmission. During the experiments, the pressures in the IFT and RIF housing were maintained at 4 Torr. The plot in Figure 3b shows the dependence of the transmitted ion current on the DC gradient using the tuning mix singly charged ions in the m/z 118−2722 range. The increase of the DC gradient from 0.3 to 9.3 V/cm resulted in 2-fold sensitivity improvement. The experimental results agree with the trends observed from ion simulations (Figure 1d). The decrease in ion transmission for the low DC field is related to the spatial broadening of the ion packets associated with thermal diffusion and Coulomb expansion effects on the drift motion.[11,27] The ion current reaches a plateau at ~9 V/cm,

dx.doi.org/10.1021/ac503564c | Anal. Chem. 2015, 87, 716−722

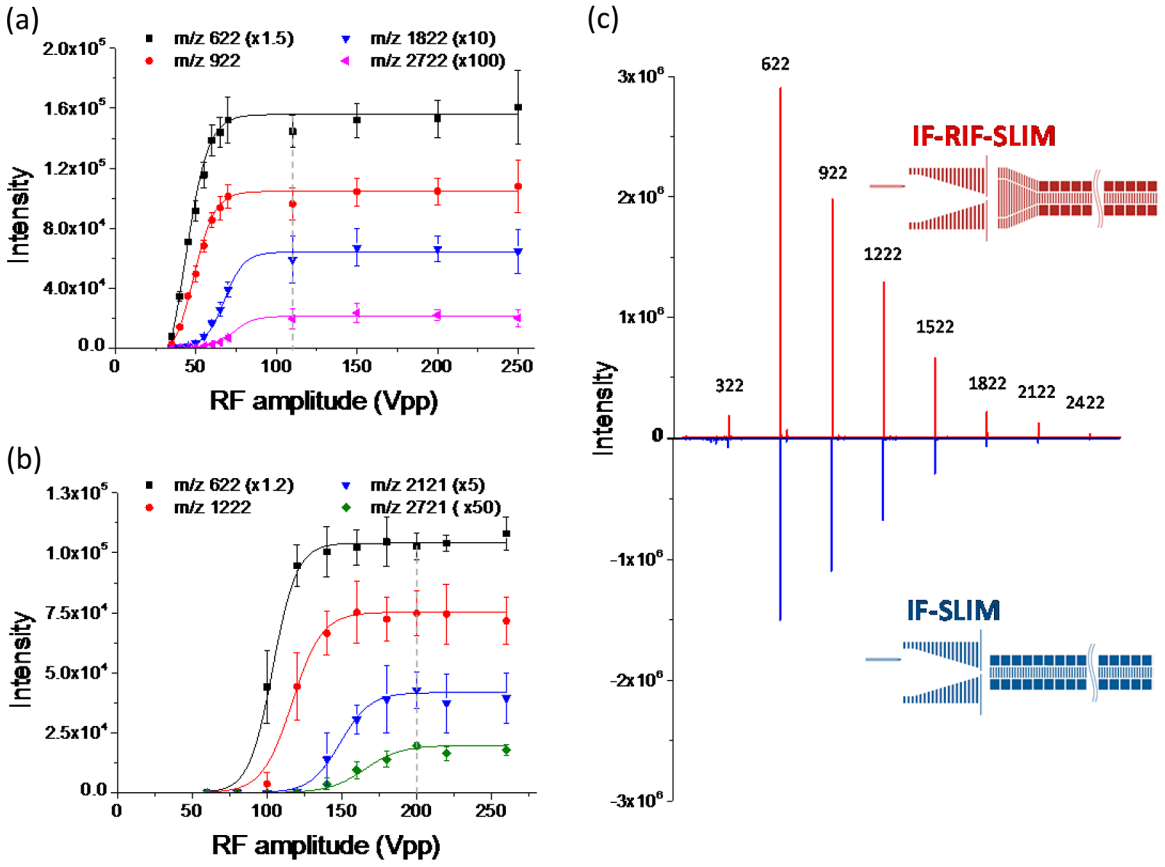

Figure 5. Optimization and performance evaluation for IFT−RIF−SLIM. The peak intensities were determined as a function of: (a) the RF amplitude for RIF and (b) the RF amplitude for the SLIM device. (c) The mass spectra of the tuning mix by an IFT−RIF−SLIM (upper) and an IFT−SLIM (lower) interface. The DC biases were optimized for the maximum ion transmission during the experiments.

suggesting a minimum requirement of 9 V/cm to avoid ion losses in the RIF.

The RIF uses different circuits for *x* and *y* electrodes allowing independent control of the DC biases at the RIF entrance and exit (Figure 2c,d). To study the effect of DC bias on the ion transmission of the RIF, the ion current was measured as a function of the guard DC biases at the entrance lens as well as at the exit lens and is shown in Figure 3c,d, respectively. Comparison of the results (Figure 3c,d) indicates that the measured current was less sensitive to the guard DC bias at the entrance lens than at the exit lens. This is attributed to the large acceptance area of RIF compared to the ion beam diameter (∼3 mm) entering RIF. Results from the ion current measurements indicate that the optimum range of guard DC bias was −10 to +10 V for the RIF entrance lens and +1 to +3 V for the RIF exit lens. The low intensities at the higher and lower DC biases resulted from ion dispersion in *y* (Figure 1c upper left) and *x* (Figure 1c lower right) directions, respectively.

RIF−SLIM Characterization. The RIF and SLIM module was interfaced with a time-of-flight mass spectrometer (model 6224 TOF-MS, Agilent Technologies, Santa Clara, CA) in order to evaluate the performance of the ESI-RIF−SLIM-TOF-MS system. Figure 4a shows the schematic of the instrument configuration used in this work. The charge collector in Figure 3a was replaced by the SLIM module followed by an exit funnel and then TOF-MS. Details of the SLIM-TOF-MS configuration have been described previously.[28] Figure 4b shows the RIF−SLIM. In this work, the source IFT was operated at RF 0.8 MHz and 180 V_{pp} while the exit funnel was operated at RF 1.2 MHz and 140 V_{pp}. The RF of the short quadrupole (Q0) behind the exit ion funnel was 124 V_{pp} at 0.8 MHz. To ensure optimal ion transmission, the distance between the RIF exit lens and the entrance of SLIM was kept at 0.76 mm which matches the distance between SLIM rung electrodes. The RF waveforms applied to RIF and SLIM were not phase locked as the effect of phase difference on ion motion at a pressure of 4 Torr is negligible. Figure 5a,b shows the peak intensities as the function of RF amplitudes for both the RIF and the SLIM module, respectively. RIF and SLIM were operated at an RF frequency of 800 kHz. The selected intensities of *m*/*z* 622 and 922 ions plateau at 70 V_{pp}, and the higher *m*/*z* ions at 1822 and 2722 required higher RF amplitudes for the optimal transmission through the RIF. Similar RF-dependent trends were observed for SLIM. For instance, the peak intensity of the *m*/*z* 2721 ion became constant at RF amplitudes higher than 200 V_{pp} (Figure 5b). The results indicate that optimal transmission of ions for the *m*/*z* range from 300 to 2700 was achieved using V_{pp} (RIF) > 120 V_{pp} and V_{pp} (SLIM) > 200 V_{pp}.

A back-to-back comparison of sensitivity for the IFT−RIF−SLIM and IFT−SLIM was performed to evaluate the performance of the new design. The optimal parameters for each arrangement was as previously determined. RIF was operated at RF of 120 Vpp at 800 kHz, DC gradient of 9.5 V/cm, and guard bias voltage of 3 V (RIF entrance) and 2 V (RIF exit). The SLIM device in the IFT−SLIM configuration was operated as follows: RF 200 V_{pp} at 800 kHz; DC gradient at 15 V/cm; DC bias at 5 V. As shown in Figure 5c, a 2-fold of

dx.doi.org/10.1021/ac503564c | *Anal. Chem.* 2015, 87, 716−722

sensitivity improvement was demonstrated using the tuning mix ion by adding the RIF compared to the conventional IFT−SLIM interface. Additionally, we did not observe any significant variation in the spectral intensity during an 11 h stability test (Figure S2, Supporting Information). The enhanced ion transmission of the IFT−RIF−SLIM is attributed to improved field continuity at the RIF−SLIM interface.

CONCLUSIONS

A rectangular ion funnel (RIF) designed, fabricated, evaluated, and shown to improve the ion introduction to a newly developed SLIM device. Ion motion simulations were used to understand and determine the optimal operating parameters for ion transmission. The RIF was fabricated using PCB technology and incorporated into a SLIM-TOF MS system for instrument performance characterization. Three operating parameters, including RF amplitude, guard electrode DC bias, and central rung electrode DC gradients, were optimized for the RIF and its interface with SLIM. The results of the performance evaluation show that the RIF−SLIM provided a 2-fold sensitivity increase and displayed an extended robust operation (i.e., high stability), without significant discrimination over an m/z 300−2700 range.

ASSOCIATED CONTENT

Supporting Information

Additional information as noted in text. This material is available free of charge via the Internet at http://pubs.acs.org.

AUTHOR INFORMATION

Corresponding Authors

*E-mail: yehia.ibrahim@pnnl.gov.
*E-mail: rds@pnnl.gov.

Notes

The authors declare no competing financial interest.

ACKNOWLEDGMENTS

The authors wish to thank Drs. Erin S. Baker, Sandilya V. B. Garimella, Jonathan T. Cox, and Aleksey V. Tolmachev for helpful discussions. Portions of this work were supported by the National Institutes of Health (NIH) NIGMS grant P41 GM103493, the Laboratory Directed Research and Development (LDRD) program at Pacific Northwest National Laboratory, and the Department of Energy Office of Biological and Environmental Research Genome Sciences Program under the Pan-omics Program. Experiments were performed in the Environmental Molecular Science Laboratory (EMSL), a U.S. Department of Energy (DOE) national scientific user facility at Pacific Northwest National Laboratory (PNNL) operated by Battelle for the DOE under contract DE-AC05-76RL0 1830.

REFERENCES

(1) Fenn, J. B.; Mann, M.; Meng, C. K.; Wong, S. F.; Whitehouse, C. M. *Science* **1989**, *246* (4926), 64−71.
(2) Hofstadler, S. A.; Sannes-Lowery, K. A. *Nat. Rev. Drug Discovery* **2006**, *5* (7), 585−595.
(3) Shen, Y.; Tolić, N.; Masselon, C.; Paša-Tolić, L.; Camp, D. G.; Hixson, K. K.; Zhao, R.; Anderson, G. A.; Smith, R. D. *Anal. Chem.* **2003**, *76* (1), 144−154.
(4) James, L. S.; Matthew, M. B.; Stephen, M. B.; John, R. E.; Richard, A. Y. Analysis of Biomolecules Using Electrospray Ionization−Ion-Trap Mass Spectrometry and Laser Photodissociation. In *Biochemical and Biotechnological Applications of Electrospray Ionization Mass Spectrometry*; American Chemical Society: Washington, DC, 1996; Vol. *619*, pp 512−564.
(5) Fenn, J. B.; Mann, M.; Meng, C. K.; Wong, S. F.; Whitehouse, C. M. *Mass Spectrom. Rev.* **1990**, *9* (1), 37−70.
(6) Crotti, S.; Seraglia, R.; Traldi, P. *Eur. J. Mass Spectrom.* **2011**, *17* (2), 85−99.
(7) Bruins, A. P. *Mass Spectrom. Rev.* **1991**, *10* (1), 53−77.
(8) Douglas, D. J.; French, J. B. *J. Am. Soc. Mass Spectrom.* **1992**, *3* (4), 398−408.
(9) Ibrahim, Y.; Tang, K.; Tolmachev, A. V.; Shvartsburg, A. A.; Smith, R. D. *J. Am. Soc. Mass Spectrom.* **2006**, *17* (9), 1299−1305.
(10) Page, J. S.; Kelly, R. T.; Tang, K.; Smith, R. D. *J. Am. Soc. Mass Spectrom.* **2007**, *18* (9), 1582−1590.
(11) Tang, K.; Shvartsburg, A. A.; Lee, H.-N.; Prior, D. C.; Buschbach, M. A.; Li, F.; Tolmachev, A. V.; Anderson, G. A.; Smith, R. D. *Anal. Chem.* **2005**, *77* (10), 3330−3339.
(12) Julian, R. R.; Mabbett, S. R.; Jarrold, M. F. *J. Am. Soc. Mass Spectrom.* **2005**, *16* (10), 1708−1712.
(13) Anthony, S. N.; Shinholt, D. L.; Jarrold, M. F. *Int. J. Mass Spectrom.* **2014**, *371* (0), 1−7.
(14) Miller, T. A. *J. Chem. Soc., Faraday Trans. 2: Mol. Chem. Phys.* **1986**, *82* (8), 1123−1135.
(15) Kelly, R. T.; Tolmachev, A. V.; Page, J. S.; Tang, K.; Smith, R. D. *Mass Spectrom. Rev.* **2010**, *29* (2), 294−312.
(16) Gerlich, D. Inhomogeneous RF Fields: A Versatile Tool for the Study of Processes with Slow Ions. In *State-Selected and State-to-State Ion−Molecule Reaction Dynamics. Part 1. Experiment*; Wiley: New York, 1992; Vol. *82*, pp 1−176.
(17) Guan, S.; Marshall, A. G. *J. Am. Soc. Mass Spectrom.* **1996**, *7* (1), 101−106.
(18) Belov, M. E.; Gorshkov, M. V.; Udseth, H. R.; Anderson, G. A.; Tolmachev, A. V.; Prior, D. C.; Harkewicz, R.; Smith, R. D. *J. Am. Soc. Mass Spectrom.* **2000**, *11* (1), 19−23.
(19) Shaffer, S. A.; Prior, D. C.; Anderson, G. A.; Udseth, H. R.; Smith, R. D. *Anal. Chem.* **1998**, *70* (19), 4111−4119.
(20) Shaffer, S. A.; Tolmachev, A.; Prior, D. C.; Anderson, G. A.; Udseth, H. R.; Smith, R. D. *Anal. Chem.* **1999**, *71* (15), 2957−2964.
(21) Baker, E. S.; Clowers, B. H.; Li, F.; Tang, K.; Tolmachev, A. V.; Prior, D. C.; Belov, M. E.; Smith, R. D. *J. Am. Soc. Mass Spectrom.* **2007**, *18* (7), 1176−1187.
(22) Clowers, B. H.; Ibrahim, Y. M.; Prior, D. C.; Danielson, W. F.; Belov, M. E.; Smith, R. D. *Anal. Chem.* **2008**, *80* (3), 612−623.
(23) Kemper, P. R.; Dupuis, N. F.; Bowers, M. T. *Int. J. Mass Spectrom.* **2009**, *287* (1−3), 46−57.
(24) Gaye, M. M.; Valentine, S. J.; Hu, Y.; Mirjankar, N.; Hammoud, Z. T.; Mechref, Y.; Lavine, B. K.; Clemmer, D. E. *J. Proteome Res.* **2012**, *11* (12), 6102−6110.
(25) Koeniger, S. L.; Merenbloom, S. I.; Valentine, S. J.; Jarrold, M. F.; Udseth, H. R.; Smith, R. D.; Clemmer, D. E. *Anal. Chem.* **2006**, *78* (12), 4161−4174.
(26) May, J. C.; Goodwin, C. R.; Lareau, N. M.; Leaptrot, K. L.; Morris, C. B.; Kurulugama, R. T.; Mordehai, A.; Klein, C.; Barry, W.; Darland, E.; Overney, G.; Imatani, K.; Stafford, G. C.; Fjeldsted, J. C.; McLean, J. A. *Anal. Chem.* **2014**, *86* (4), 2107−2116.
(27) Siems, W. F.; Wu, C.; Tarver, E. E.; Hill, H. H., Jr.; Larsen, P. R.; McMinn, D. G. *Anal. Chem.* **1994**, *66* (23), 4195−4201.
(28) Webb, I. K.; Garimella, S. V. B.; Tolmachev, A. V.; Chen, T.-C.; Zhang, X.; Norheim, R. V.; Prost, S. A.; LaMarche, B.; Anderson, G. A.; Ibrahim, Y. M.; Smith, R. D. *Anal. Chem.* **2014**, *86*, 9169−9176.
(29) Webb, I. K.; Garimella, S. V. B.; Tolmachev, A. V.; Chen, T.-C.; Zhang, X.; Cox, J.; Norheim, R. V.; Prost, S. A.; LaMarche, B.; Anderson, G. A.; Ibrahim, Y. M.; Smith, R. D. *Anal. Chem.* **2014**, *86*, 9632−9637.
(30) Garimella, S. V.; Ibrahim, Y. M.; Webb, I. K.; Tolmachev, A. V.; Zhang, X.; Prost, S. A.; Anderson, G. A.; Smith, R. D. *J. Am. Soc. Mass Spectrom.* **2014**, *25*, 1890−1896.
(31) Tolmachev, A. V.; Webb, I. K.; Ibrahim, Y. M.; Garimella, S. V. B.; Zhang, X.; Anderson, G. A.; Smith, R. D. *Anal. Chem.* **2014**, *86*, 9162−9168.

(32) Kelly, R. T.; Page, J. S.; Luo, Q.; Moore, R. J.; Orton, D. J.; Tang, K.; Smith, R. D. *Anal. Chem.* **2006**, *78* (22), 7796−7801.